Int. J. Heat Mass Transfer. Vol. 30, No. 11, pp. 2305–2317, 1987
Printed in Great Britain

0017–9310/87 $3.00 + 0.00

Local liquid–solid mass transfer measurement in a trickle film flow model using an electrochemical technique

PAO C. CHAU

Department of Applied Mechanics and Engineering Sciences (Chemical Engineering), University of California, San Diego, CA 92093, U.S.A.

(*Received* 5 *November* 1986 *and in final form* 5 *April* 1987)

Abstract—A two-dimensional trickle film flow model consisting of a vertical column of horizontal rods is used to provide the liquid–solid mass transfer characteristics of a gas-continuous and fully wetted film flow trickle bed reactor. Local and average liquid–solid mass transfer rates are determined with the limiting current technique. Local Sherwood number variation with angular position is measured for $400 < Re < 2000$. With a unique method of manipulating electrochemical mass transfer measurements, the existence of two vortices behind a flow separation is revealed.

INTRODUCTION

A TRICKLE bed catalytic reactor consists of a packed column with gas–liquid cocurrent downflow. The reactor is commonly used in the petroleum industry and in oxidation reactions of dissolved organic acids. Interests in the study of various aspects of trickle bed reactor remain keen and current [1–4]. The hydrodynamics of a trickle bed reactor is complicated. Various operating regimes are classified as trickle, ripple, pulse and dispersed bubble flows [5]. Multiplicity of hydrodynamic regimes has also been observed [6].

As a multiphase reactor, considerations of gas–liquid and liquid–solid mass transfer rates cannot be neglected. Liquid–solid mass transfer resistance may become important when the reactions are relatively fast. Liquid–solid mass transfer coefficients in each hydrodynamic flow regime have been subjected to repeated studies [7–13]. Most of the liquid–solid mass transfer measurements are based on dissolution of a sparingly soluble packing material, e.g. benzoic acid. The result is the overall mass transfer coefficient of the reactor.

As an attempt to probe the mass transfer characteristics of the reactor on a more detailed level, local mass transfer rates were measured in several studies utilizing an electrochemical limiting current method. The basis of the method is that the rate of an electrochemical reaction is dependent on the applied electrode potential. The electrochemical reaction rate on the electrode surface can be adjusted such that it is entirely mass transfer rate limited. A typical electrochemical system is the reduction of ferricyanide ions under polarographic conditions. Mass transfer rates to an individual packing particle [14, 15] or a small stack of spheres [16] in a trickle bed have been obtained with the limiting current method.

With a microelectrode around 0.5–0.6 mm in diameter, local mass transfer rates along the particle surface can also be measured. Such a technique was used in a randomly packed and a regularly packed cubic array column with fairly large spheres (25.4–76.2 mm diameter) and single liquid phase flow [17, 18]. The observed results illustrated complicated flow structures present in both single and multiphase flow packed columns. The measured mass transfer rate is highly dependent on whether the electrode surface is wetted by the liquid. Thus the electrochemical technique is best applied to the trickle film flow regime in which the liquid phase flows down the column packing as a thin liquid film and the gas phase is continuous.

The objective of our work is to study the mass transfer characteristics of a trickle film flow on a more refined scale than Rao and Drinkenburg [15] and Delaunay *et al.* [16]. In particular, we intend to measure the local variation of mass transfer coefficients along the particle surface. With a unique combination of measurements which is explained in the procedures, we can probe the actual fluid field quite precisely close to the surface under trickle film flow conditions. The scale of the particles is similar to those used in industrial reactors, i.e. around 6 mm. From the results of the earlier studies [15–18], it is apparent that we would need a better defined condition than an actual packed column [17, 18]. To achieve our goals, a much simplified trickle flow model is used. The experimental model consists of a single rod column with cocurrent gas flow on both adjacent sides. This simple configuration obviously cannot simulate other hydrodynamic regimes of a trickle reactor, but suffices for the trickle film flow regime under consideration. The model also provides a good experimental comparison to the theoretical trickle flow model based on periodically constricted tubes [19]. Our results should also provide complementary observations to heat transfer of isolated cylinders in crossflow [20].

NOMENCLATURE

D	molecular diffusivity
k	local mass transfer coefficient
k_1	isolated mass transfer coefficient
L	half circumference length of rod surface
Sh	Sherwood number
Sc	Schmidt number
Re	Reynolds number of liquid film
Re_p	Reynolds number based on a packed column
x	position of the point electrode.

Greek symbols

Γ	liquid mass flow rate
ε	void fraction of packed bed
θ	angular position on the cylindrical surface
ν	kinematic viscosity
τ_w	local shear stress.

EXPERIMENTAL METHODS

Apparatus

The trickle flow model (Fig. 1) is a vertical column of 20 rods, each 6 mm in diameter and 0.16 m in length. The rods are encased in a plexiglas box with moveable side walls. At the top of the rod column, a stainless steel strip (0.7 mm thick) guides the liquid flowing down from the distributor slit. At the bottom, the collector is divided into nine compartments. The segmented collector allows the flow distribution along the rods to be checked. Air is fed into the device from distributors on both side walls. The air flow entering the elongated distributor is broken up by a baffle and fed into the air gap adjacent to the rod column through a series of 1.6 mm diameter holes. The air originates from house compressed air which passes through a humidifier and a rotameter (maximum capacity 3.03 l s^{-1}).

A centrifugal pump with a polypropylene housing delivers the liquid from a 20 l polyethylene reservoir through a rotameter (maximum capacity 0.17 l s^{-1}) into two manifolds leading to the liquid feed distributors. A recycle loop which bypasses the apparatus and allows prior makeup of electrolyte solution in the reservoir is included. A stainless steel cooling coil in the reservoir maintains the temperature within 0.5°C of 25°C. A stainless steel sparger is placed in the reservoir. Nitrogen is used to purge the electrolyte of oxygen throughout the duration of each experiment.

Electrodes

Both anode and cathode are fabricated as sections of the rod column. Three different cathodes are used: a small point electrode a rectangular electrode and a rod electrode. The cathode is located at the center of the fourth rod from the bottom. The anode consists of segments of 10 and 2 rods above and below, respectively, the rod containing the cathode which is separated from the anode by two glass rods. The anode is fabricated from brass rods, silver-soldered together at the ends and plated with bright nickel.

Both the point and rod electrodes are constructed on a single piece of nickel with a 0.86 mm fin edge 6 mm in diameter and tapered ends (Figs. 2(a) and (b)). The narrow fin edge is the rod cathode electrode. A 127 μm diameter platinum wire with a thin insulating coating of epoxy is threaded through drilled holes and

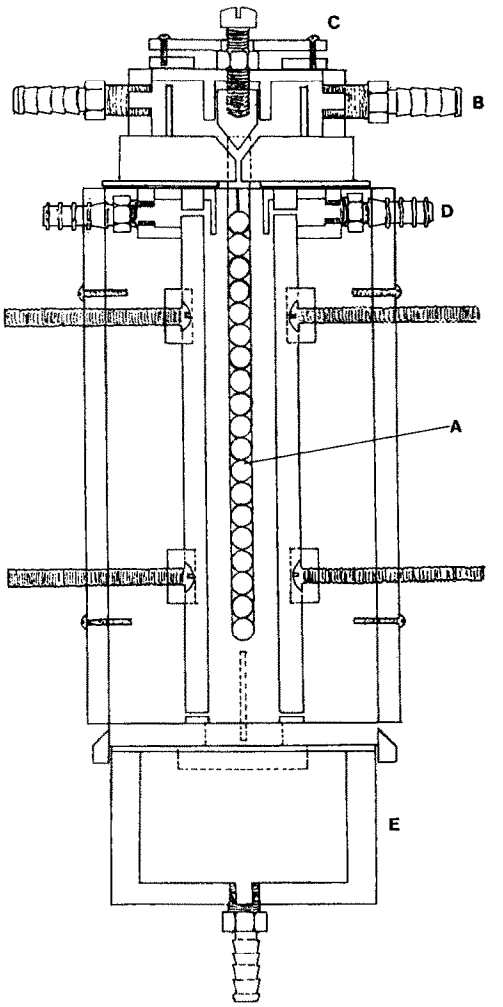

FIG. 1. Schematic end view of the trickle flow rod column: A, the rod column; B, liquid inlet; C, flow distributor; D, air inlet; E, collector.

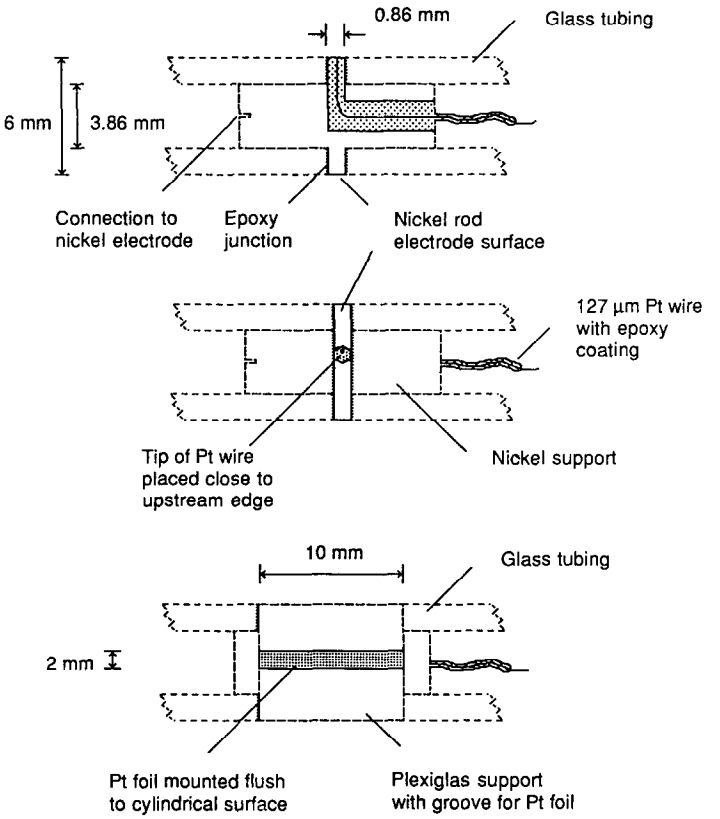

FIG. 2. Schematic of the electrode configurations: (a) point and rod electrode, side section; (b) point and rod electrode, top view; (c) rectangular electrode, top view.

its tip is mounted flush with the rod electrode. Two 6 mm o.d. pyrex glass tubings are slipped onto the tapered ends and cemented in place with epoxy. For the rectangular electrode, it is a piece of 10×2 mm and 25 μm thick platinum foil mounted flush on a piece of 6 mm diameter plexiglas (Fig. 2(c)).

The anode is held at ground potential and the cathode is kept at a negative potential by a potentiostat. The electrode current is converted to a voltage signal. With the rectangular cathode or the rod cathode, the fluctuations of the voltage signal from the amplifier were usually insignificant and readings were taken using a low pass capacitor filter. With the small point electrode, the average voltage signal from the amplifier was integrated over a period of 30–90 s to obtain the time average.

Procedure

All experiments are performed with 1 M NaOH as the supporting electrolyte, and equimolar concentrations of potassium ferricyanide and ferrocyanide (10 mM) and the solution is discarded after each run. At 25°C, the solution density is 1045 kg m^{-3}, the viscosity is 0.0126 poise, the diffusivity of ferricyanide ion is 6.65×10^{-10} m^2 s^{-1}, and the Schmidt number is 2071. The liquid flow rates are always varied from high to low, to ensure uniform wetting at the lower flow regime and conform to typical reactor startup to achieve trickle film flow [6].

To explore the nature of the fluid flow and mass transfer on the surface of the cylindrical surface, two different sets of experiments are required. An illustration is provided in Fig. 3.

(1) Measurements of local mass transfer coefficient, k, with both the rod nickel surface and the point electrode activated as cathode. Thus, apart from the thin epoxy ring around the point electrode, essentially the entire fin surface is active. Only the current collected from the point electrode is measured.

(2) Measurement of *isolated* mass transfer coefficient, k_i, with only the point electrode acting as an isolated cathode, i.e. active surface for mass transport. Here the rest of the fin (rod) surface is electrochemically inactive.

The difference between situations 1 and 2 is that the point electrode in the second experiment is always at the leading edge of a developing concentration boundary layer for all angular positions. This is clearly not the case in the first situation. The local mass transfer coefficient, obtained with the entire nickel fin electrode also active, can only be either equal to or less than the value obtained from the isolated electrode. Hence, the resulting point electrode mass flux should be higher under the isolated electrode condition than the corresponding flux in the first experiment with a uni-

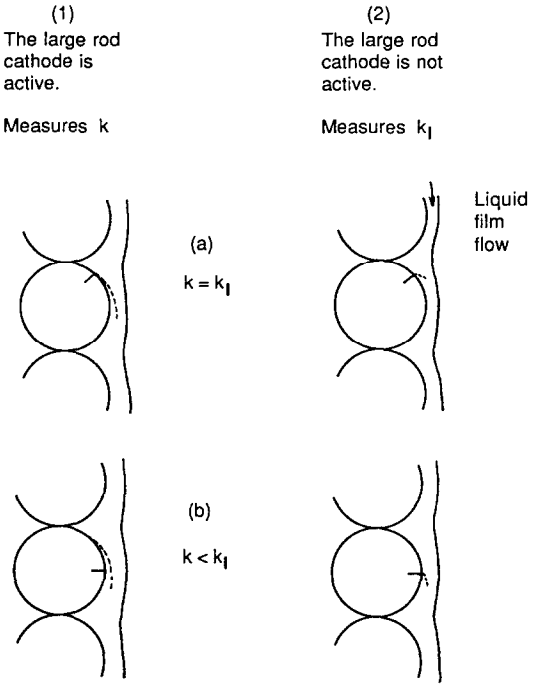

FIG. 3. Experimental scheme for determining the development of the boundary layer on the cylindrical surface. (1) Measurement of local mass transfer coefficient by the point electrode inside concentration layer developed by the large rod electrode. (2) The point electrode is always at the leading edge of a developing concentration boundary layer.

formly active fin. In general, $k_l/k \geqslant 1$.

When the experimental ratio k_l/k is unity at some position x (angle θ), we infer that the fluid flow in the region around x is bringing essentially fresh bulk fluid to the active point electrode. In such a case, the point electrode is situated at a stagnation point at the front, or for recirculation zones, in the rear of the cylinder in both experiments. Here the history of fluid flow on the surface has no effect since the stagnation point receives fresh bulk fluid. Further downstream from the stagnation point, the result of the local mass transfer experiment will be progressively lower than that for the isolated electrode, since the electrode in the former experiment is situated well into a developed concentration boundary layer. At a flow separation point still further down the surface, the ratio k_l/k should be largest. With an isolated electrode, fresh solution is brought to the separation point from both upstream and downstream. However, in the local mass transfer measurements, the point electrode, surrounded by the active rod electrode, is receiving a fluid previously depleted by both the upstream and downstream portions of the rod electrode. These events lead to a large k_l, small k, and thus a maximum k_l/k. Similarly a stagnation point resulting from a closed recirculation behind a separation should also exhibit a ratio k_l/k of unity. A plot of k_l/k vs position on the surface together with another plot giving the absolute mass transfer rate would allow us to interpret the refined details of fluid flow and mass transfer on the surface.

The mass transfer rate in the second experiment with the isolated electrode is very sensitive to the fluid flow and can be used to determine the local shear stress on a surface [17]. For situation 1, the leading edge of a developing concentration boundary layer coincides with that of a developing hydrodynamic boundary layer. Beyond the leading edge, the hydrodynamic boundary layer will become very much thicker than the concentration boundary layer because of the high Schmidt number of the liquid medium.

In addition to the above two experiments, the average mass transfer coefficient is also measured with the rod electrode. The point electrode is moved to either the very top ($\theta = 0$) or the very bottom ($\theta = \pi$) position. The rod surface alone acts as the cathode. Measurements of the mass transfer coefficient with the rectangular cathode are used to test the influence of electrode size.

RESULTS AND DISCUSSION

The variations of local mass transfer and calculated shear stress with the liquid Reynolds number and angular position are presented here. The patterns evident in these results lead to our interpretation of the flow field and boundary layer development on the cylindrical surface of the model trickle reactor. Results of mass transfer from the experimental model are compared with actual trickle flow reactors.

Local mass transfer profiles

The local mass transfer profiles are represented by the plots (Fig. 4), at constant Re, of Sh vs angular position along the surface. The mass transfer coefficients are reported in terms of the Sherwood number, $Sh = k\,dp/D$, using the diameter of the rods, dp, and the diffusivity, D, of the ferricyanide ion. For later comparison with simple falling film flow and trickle bed mass transfer correlations, the mass transfer coefficients are correlated with

$$Sh = a\,Re^n\,Sc^{1/3} \tag{1}$$

where Sc is the Schmidt number and Re is the liquid film Reynolds number, defined [21] as

$$Re = 4\Gamma/v \tag{2}$$

where Γ is the mass flow rate and v the kinematic viscosity.

We first consider some characteristic features. Illustrative $Sh\,Sc^{-1/3}$ vs Re cross-plots of Fig. 4 at several selected angular positions are shown in Fig. 5. These plots exhibit a laminar to turbulent transition around $Re = 1000$. (The corresponding transition with planar films occurs at $Re = 1080$.) The smoothness of the shift is characteristic of falling liquid films [22].

In the laminar flow regime, $Re < 1000$, most of the

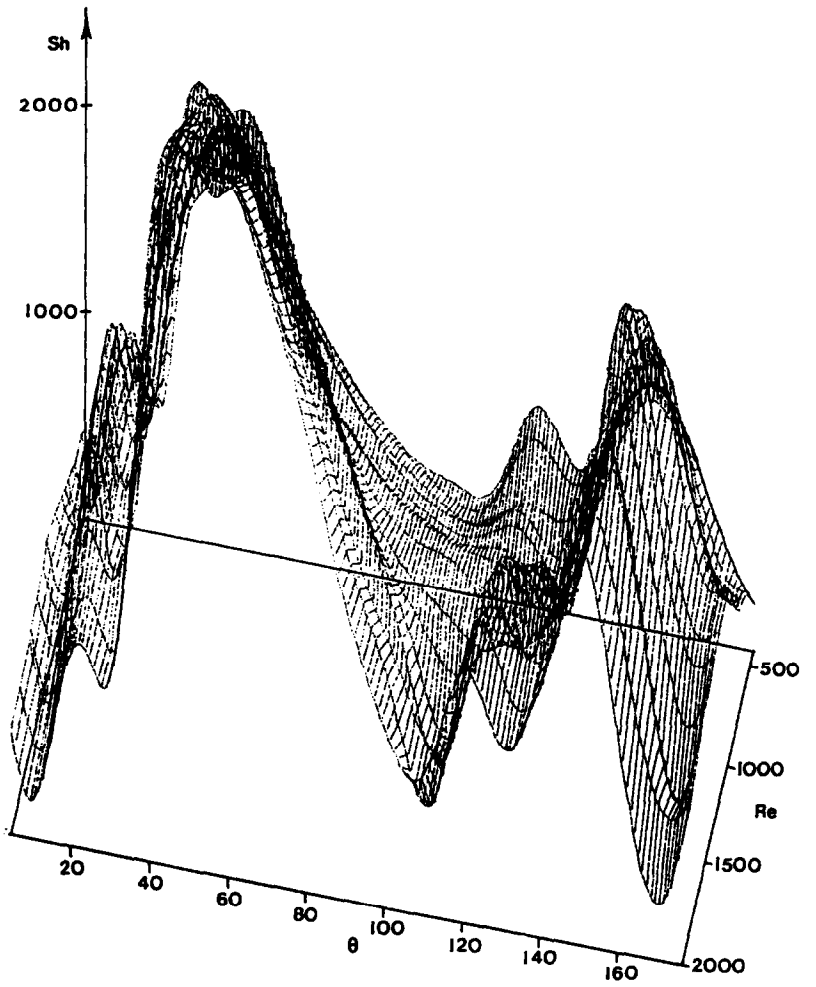

FIG. 4. The profiles of local mass transfer coefficient in terms of *Sh* along the cylindrical surface. The scan of the angular positions is from 5° to 175° on the surface.

angular positions indicate only a slight increase in mass transfer rate with flow rate. The exceptional location occurs in the region from 100° to 140° (e.g. the 120° shown) which displays a reverse trend. Thus, within certain angular positions and Reynolds number ranges, the local mass transfer *decreases* with increasing *Re*.

This anomalous behavior is more common in the turbulent flow regime where the majority of the angular positions exhibit diminished mass transfer rates with increased *Re*. Here only the region 60°–90° indicates the normal trend of increasing mass transfer rate with *Re*. At 50°, there is an exceptionally long transition region to turbulent flow, and at 40° (Fig. 5), the transition is so long that this position never attains fully developed turbulent flow.

The values of a and n in correlation (1) are summarized in Table 1. It is striking to note that the Reynolds number dependence, n, is small. The value of n for overall mass transfer (laminar flow) is 0.24, about half that of simple falling film flow ($n = 0.5$). The local dependence varies from negative in the odd regions to 0.45. Before interpretation of the data, it is necessary to refer back to Fig. 4.

All the profiles in Fig. 4 have irregular peaks dispersed along the surface between the two contact points (0°, 180°). Nevertheless, the results are observed to possess a fairly orderly change in pattern. Four local maxima, two minor and two major peaks, can be identified in each *Sh* profile. The first minor peak occurs at 20° and the second minor peak at 120°. The first major peak occurs at the position 50° for laminar flows, and is less well defined in the turbulent regime, where this peak is found in the region 40°–60°. The second major peak occurs invariably at 155° and 150° for laminar and turbulent flows, respectively.

There are several exceptions to the above pattern. The second minor peak disappears in the range of $Re = 800$–1000, and the peak is shifted to 130° in the range of $Re = 1200$–1300. The first minor peak is shifted slightly to 25° and is not very prominent at flow rates higher than $Re = 1900$.

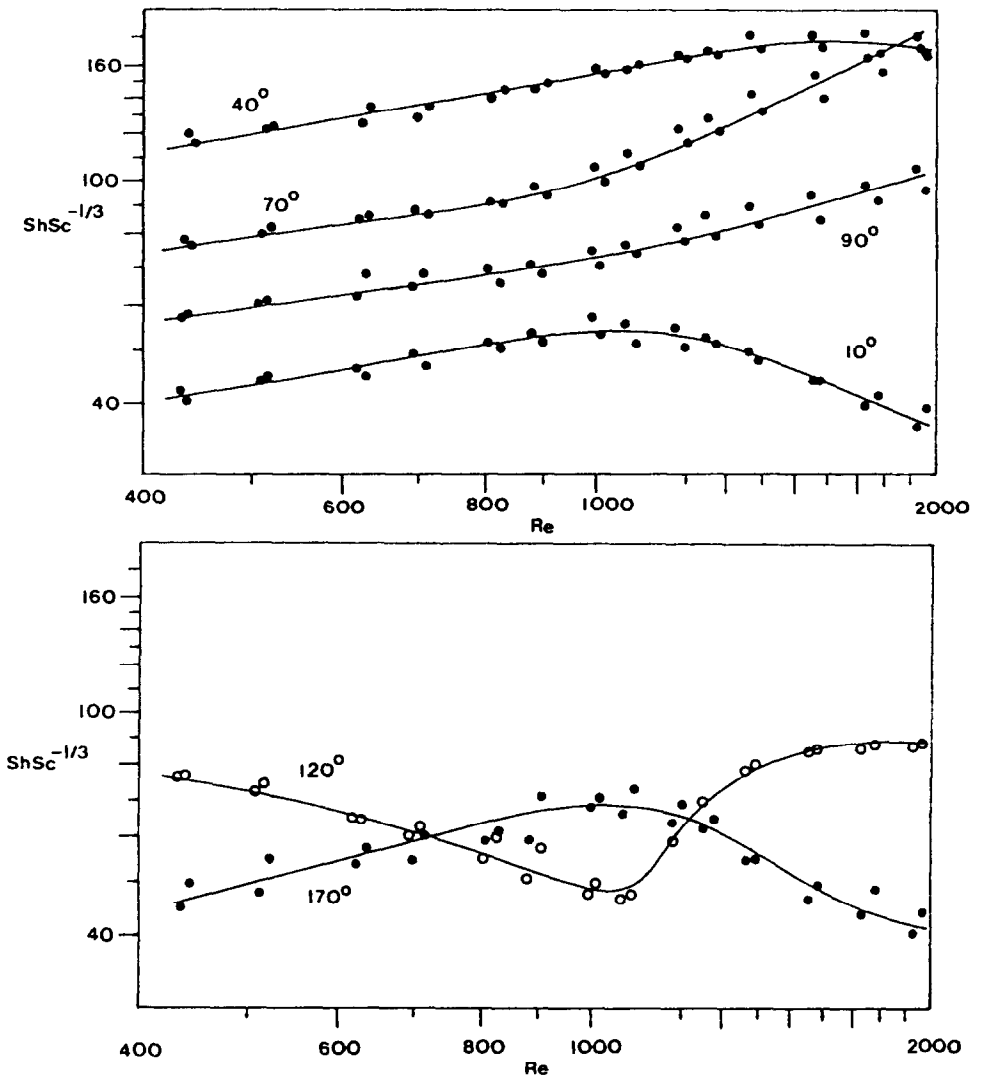

FIG. 5. Dependence of the local mass transfer rate on Re at several selected angular positions.

The most important observation is that the positions of the peaks remain at roughly the same locations over a very wide range of flow rates. It is logical that some regions close to the surface, in particular those near 0° and 180°, are not very sensitive to the external bulk flow. As a consequence, established patterns remain so even in the bulk film turbulent regime. For flow rates above $Re = 1100$, we note that the Sh curves for higher flow rates lie *below* those for lower flow rates in the regions of the first and second minor, and of the second major peaks. This behavior is a direct consequence of the abnormal feature discussed earlier.

Local shear stress estimation

With the isolated point electrode, we expect that for high Schmidt number and appreciable Re, the isolated electrode mass transfer coefficient is proportional to the cube root of the local shear stress in the region along the surface where a laminar hydrodynamic boundary layer exists [23]. From Acrivos' analysis [23], the local Sherwood number is

$$Sh(x) = \sqrt{Re}\left(\frac{Sc}{9}\right)^{1/3} \frac{\sqrt{(\beta(x))}}{\left[\Gamma(4/3)\int_{x^*}^{x}\sqrt{(\beta(x))}\,dx\right]^{1/3}} \tag{3}$$

where β is the dimensionless velocity gradient on the solid surface and x^* is the starting position of the region where mass transfer occurs. With the assumption that the variation of shear stress is negligible over the small point electrode, we can write [17]

$$\tau_w = \left(\frac{2\Gamma(4/3)k_1}{3}\right)^3 \frac{9x_e\mu}{D^2} \tag{4}$$

Table 1. Liquid flow rate dependence of local Sherwood number as obtained by the point electrode. Only angular positions every 10° are summarized here. The average value is obtained by the rod electrode

Position (deg)	a	n
(a) Laminar flow, $Re < 1000$		
Average	11.6±1.2	0.24±0.03
5	22.0±1.2	0.14±0.03
10	6.1±1.3	0.32±0.03
20	42.0±1.0	0.11±0.03
30	15.4±1.2	0.30±0.03
40	13.7±1.1	0.35±0.02
50	9.2±1.2	0.40±0.03
60	11.4±1.1	0.34±0.02
70	15.8±1.2	0.26±0.02
80	22.3±1.1	0.18±0.02
90	12.6±1.3	0.25±0.03
100	12.9±1.1	0.24±0.01
110	42.2±1.2	0.05±0.03
120	Negative exponent	−0.53±0.04
130	Negative exponent	−0.24±0.08
140	50.4±1.1	0.07±0.02
150	13.6±1.4	0.31±0.06
160	4.6±1.2	0.45±0.02
170	29.3±1.3	0.10±0.04
175	30.3±1.4	0.09±0.06
(b) Turbulent flow, $Re > 1000$		
Average	60.0±1.1	0.01±0.01
5	Negative exponent	−0.20±0.01
10	Negative exponent	−0.68±0.12
20	Negative exponent	−0.75±0.21
30	Negative exponent	−0.95±0.23
40	Not quite reach turbulent flow	
50	Barely reach turbulent flow	
60	16.5±1.8	0.32±0.08
70	1.2±1.8	0.66±0.08
80	1.3±1.5	0.62±0.06
90	5.3±2.2	0.39±0.11
100	Negative exponent	−0.24±0.16
110	Separation region	
120	Separation region	
130	Negative exponent	−0.35±0.12
140	8.7±1.7	0.31±0.07
150	Negative exponent	−0.34±0.10
160	Negative exponent	−1.10±0.10
170	Negative exponent	−0.68±0.15
175	Negative exponent	−0.45±0.06

where τ_w is the local wall shear stress, k_l the isolated point electrode mass transfer coefficient, and x_e the electrode length.

The τ_w profiles calculated are plotted in Fig. 6. These profiles are used as a *qualitative* analytical aid to identify separation points and stagnation points or development of boundary layer flow. The shear stress is supposedly zero at a separation point and a stagnation point, and very large near the leading edge of a developing boundary layer flow. However, we stress the point that equation (4) only provides qualitative information as the analysis is restricted to regions of laminar boundary layer flow. Because the experimental measurements are taken prior to any knowledge of the flow behavior, the calculation is applied to all data points. The shape of these shear stress profiles is best compared with the local mass transfer profiles. The positions of the local maxima in mass transfer necessarily correspond to the maxima in the shear stress curve.

There are several distinctive features in the shear stress profile. At position 120° where the second minor mass transfer peak appears (Fig. 4), the shear stress curve exhibits a sharp decrease in shear stress. The drop indicates that the position is just behind a separation point (velocity gradient is zero), and the slight increase in mass transfer at the position 120° is due to a tangential back flow generated by the vortex behind a separation point.

At high flow rates ($Re > 1200$) the separation point moves up to 100° and the decline in shear stress due to the separation point is evident in the large drop in shear stress in the forward half of the cylindrical surface, 60°–90°.

The decrease in shear stress along the front half of the surface, 60°–90°, is gradual in the laminar flow regime. Below $Re = 600$, there is only a slight decrease in shear stress along the surface. The shear stress increases abruptly after the flow passes the separation point and declines sharply thereafter. It should be noted that the isolated electrode mass transfer rate is the measured quantity; the peak in this measurement near the separation point reflects only the enhanced mass transfer due to the acceleration of the recirculation from the back side; i.e. behind the flow separation. The shear stress analysis leading to equations (3) and (4) is of course invalid here. The magnitude of the 'shear stress' immediately after the separation point is approximately 40 g cm^{-1} s^{-2}, and is independent of Re. This behavior probably accounts for the increase in 'shear stress' just after the separation point in the lower flow rates.

In the region from 30° to 60°, and with $Re > 100$, the shear stress does not increase smoothly as in the mass transfer profiles. There is a slight notch at 50°. At this position, it is very likely that the external turbulent flow intersects the laminar secondary flow from the separation vortex and disrupts the boundary layer flow and the shear stress slightly.

In the turbulent flow regime ($Re > 1400$) the maximum shear stress moves down to 70°. This observation corresponds to the slight shift in the first major mass transfer peak and suggests a diminished region of boundary layer flow on the surface.

Interpretation of the boundary layer development

The ratio of the measured mass transfer coefficient from the isolated electrode to that of the measured local mass transfer coefficient, k_l/k, is plotted in Fig. 7. In the region 40°–140°, the ratio k_l/k rises from unity to more than two and then drops down to one beyond 120°. This peak region becomes progressively smaller and narrower as the flow regime becomes turbulent. In the highly turbulent regime (e.g. $Re >$

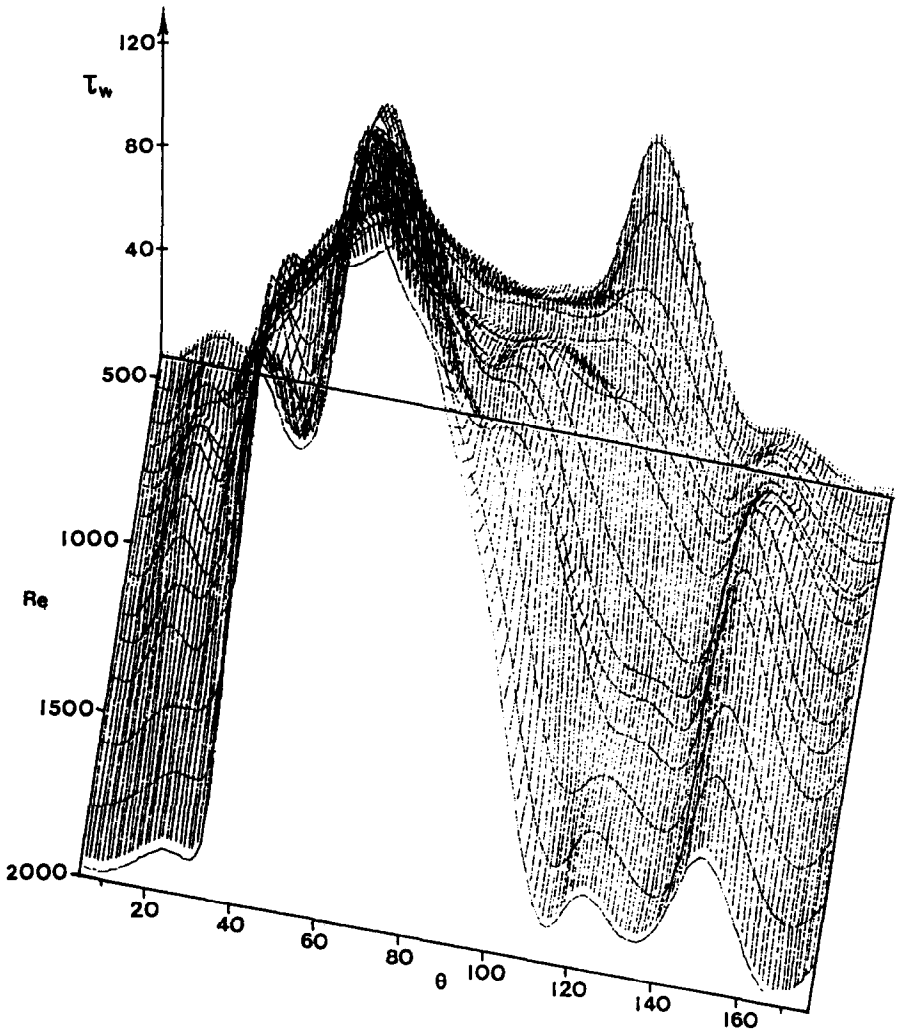

FIG. 6. The τ_w (g cm^{-1} s^{-2}) profiles along the cylindrical surface at different *Re* obtained with the isolated point electrode.

1900), the ratio k_1/k does not increase from unity until $\theta = 60°$, and it drops back to one at 120°.

The general features of the local mass transfer profiles and the value of k_1/k are illustrated in Fig. 8, together with the interpretation of the flow pattern near the surface. Let us first review the general pattern of changes. The profiles illustrated are typical of laminar flow and the arrows indicated the shift in the pattern as the flow becomes turbulent. In the laminar flow region, the first major mass transfer peak occurs at 40°–50°. Since the ratio k_1/k is unity around 40°, the first major peak in the mass transfer profiles is the result of a developing concentration boundary layer, beginning at a flow stagnation point. This first major peak shifts toward 60° in turbulent flow; similarly the ratio k_1/k does not deviate from unity until $\theta = 50°$–60° for *Re ca.* 1900.

Since the isolated electrode is very sensitive to the flow field and thus provides a measure of the local wall shear stress, it is reasonable to assume that where k_1/k is unity, the leading edge of the development of the hydrodynamic boundary layer coincides with that of the concentration boundary layer (region 40°–60°).

As the ratio k_1/k increases from unity, the local Sherwood number and local shear stress each decreases along the surface. When the fluid flow moves away from the stagnation point (and the leading edge of the boundary layer development), a positive pressure gradient will retard the fluid flow close to the surface, eventually leading to flow separation.

The second minor and second major peaks are results of flow separation. In the laminar flow regime, the ratio k_1/k approaches its maximum value near the 110°–120° region, corresponding to the minimum in the mass transfer profiles. This observation, together with the sharp drop in local shear stress in the 120° region (earlier for $Re < 700$), indicates a flow separation point. Examination of the location of minimum shear stress (or the maximum in the ration k_1/k) for different Reynolds number in Fig. 6 (or 7) shows

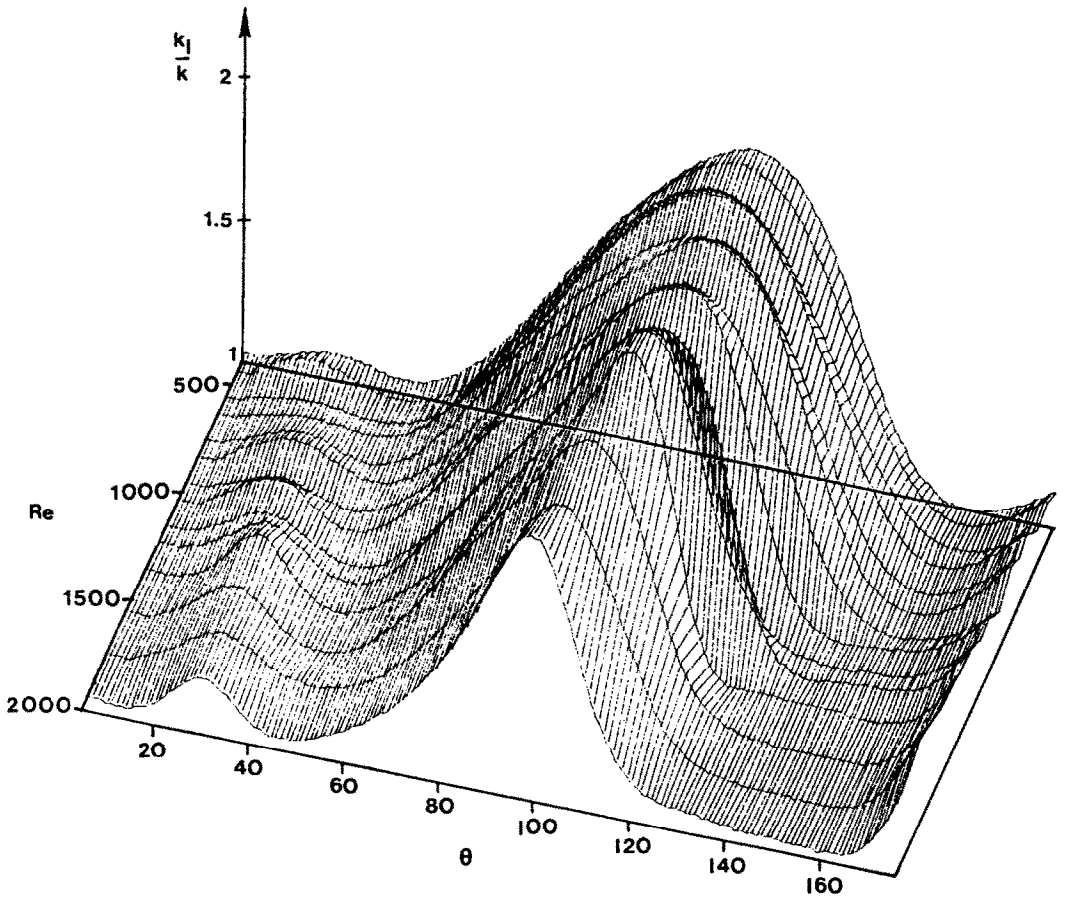

FIG. 7. The surface profiles of the ratio of the mass transfer coefficients of the isolated electrode to the local electrode, k_l/k.

that the separation moves slowly from under 110° to 120 in the laminar regime, and moves back to 100° in the turbulent flow regime.

The Blasius series solution for laminar flow past an isolated cylinder predicts flow separation at 110° [24]. Our separation points in laminar flow are between 100° and 120°, indicating that the upstream and downstream cylinders have the most influence at the lowest Reynolds numbers used.

The positions of the peaks at 120° and 150° in the mass transfer profiles probably exist at the two ends of a separation vortex (Fig. 8, vortex I). The leading edge of the backflowing vortex is at 150°, corresponding with the value of k_l/k being unity. The minor peak at 120° is likely to be a result of some small scale local mixing between the separation point and the back flow from 150°. From the presumed direction of the flow directions (Fig. 8), a small separation vortex is unlikely to occur at 120°. Accordingly, the entire k_l/k peak from 40° to 140° arises from two different situations—a boundary layer of the primary flow from 40° to the separation point, and a recirculation vortex behind the flow separation.

Near the crevice between the contact point of two rods (180°), k_l/k increases slightly from one. In the mass transfer profiles, the mass transfer rate does not appear to approach a diminishing value in the region very close to the contact points. The mass transfer rate also exhibits a very slow regular fluctuation with time (not shown). Thus it is probable that some form of convective flow, likely close to the creeping flow regime, exists in the crevice. However, the data are not adequate to deduce the exact nature of flow in this region.

The ratio k_l/k increases slightly in the region 20°–35° which corresponds with the first minor peak at 20°. The only plausible explanation is that there are two vortices behind the separation. The peak at 20° arises from a smaller vortex (Fig. 8, vortex II) behind the major vortex which gives rise to the second major peak in the preceding rod. The minimum in the mass transfer profile at 25°–30° occurs where the two vortices meet (i.e. at flow separation). Immediately downstream, we encounter the stagnant point and the initiation of boundary layer flow development near 40°.

Consistency test

The consistency of the point electrode results is checked with that of the average mass transfer

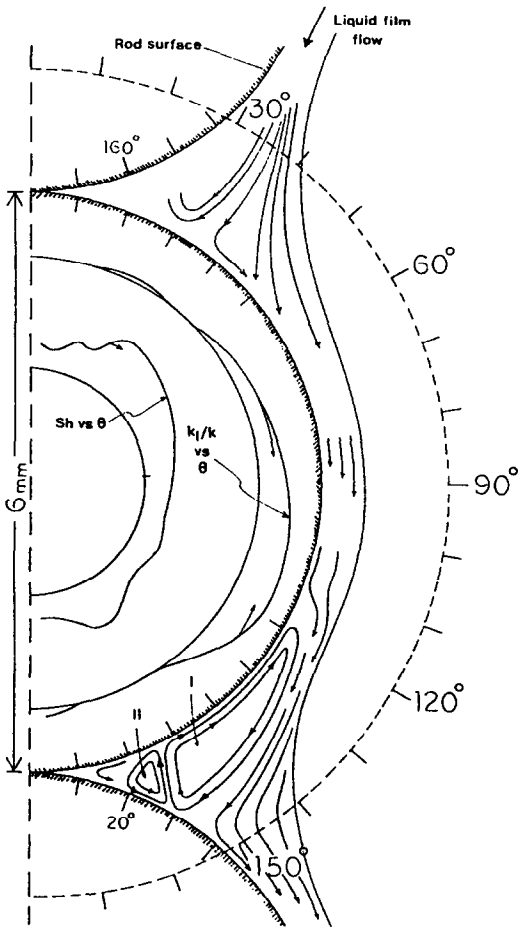

FIG. 8. Flow map close to the cylindrical surface illustrating the vortex formation.

coefficient, obtained from the large nickel electrode. For perfect agreement

$$\int_0^{\pi} \frac{Sh(\theta)}{\overline{Sh}} d\theta = 1$$

where $\overline{Sh}$ is the average Sherwood number. However, integration of all the local mass transfer rates results in a factor of 1.6 for all values of the Reynolds number. It is apparent that the average mass transfer rate obtained from the local mass transfer experiment is higher than that of the average mass transfer experiment.

This apparent discrepancy is due to the presence of the inert epoxy ring around the electrode. The concentration of the solute is not being depleted by diffusion to the epoxy layer. Thus at the edge of the electrode, the transport of solute tangentially enhances the diffusion in the normal direction, leading to a higher mass flux. The electrode region in which the contribution of the tangential transport is important is the *relaxation area* [25]. The small point electrode is situated entirely in the relaxation area. The resulting effect is a 1.6 times larger effective electrode area, corresponding to an effective electrode diameter 1.23 times larger than that of the actual platinum wire.

This edge effect of the relaxation area is expected to be less important with larger electrodes. Indeed, integration of the local Sherwood number with the rectangular electrode results in average values in good agreement with that from the large electrode.

The data of Jolls and Hanratty [17] also exhibited a higher than average mass transfer rate. The size of their electrode is 510 μm. Thus an effective area higher than the simple geometric value appears to be a common feature of microelectrodes.

Laminar bulk flow: the weak dependence of mass transfer on Reynolds number

The trickle flow model behaves quite differently from an isolated sphere or cylinder, particularly the dependence on the film *Re* is extremely weak. We first discuss the relative contribution of surfaces to mass transfer.

For flow over a single sphere or cylinder, the back half of the surface contributes significantly to the overall mass transfer in the turbulent regime. The ratio of mass transfer coefficients in the forward hemispheres to those in the backward half *decreases* from 3 in laminar flow to slightly above 1 in the turbulent regime in a single phase flow packed bed [17].

However, with the trickle rod column and as the flow becomes turbulent, the second half of the rod ($\theta > 90°$) does not provide progressively higher contributions to the overall mass transfer. The fractional contribution of the first half ($\theta < 90°$) of the surface actually increases from 0.54 at $Re = 434$ to 0.61 at $Re = 1740$ (Fig. 9).

For an isolated non-streamline body, the turbulent wake behind a separation extends to the back side and helps to bring in more fresh fluid into the separation vortices. As the separation point moves forward and turbulence in the wake increases, the mass transfer contribution of the back half of the body likewise increases.

In the trickle rod column, the rods are in contact with each other at 0° and 180°. This geometry prohibits a separation wake from growing and bringing in fresh solution to the entire back side. Instead, the resulting secondary flows are recirculating vortices with closed streamlines behind the separation. As the flow becomes more turbulent, the separated boundary layer tends to form a jet that flows into the bulk stream [26]. This behavior evidently leads to a lower relative mass transfer contribution from the main flow to the vortices, and in turn to the solid surface between 90° and 180°.

In this respect, the reverse trends in the local mass transfer rates with increasing *Re* in Fig. 5 are very good indicators of these recirculating vortices. The existence of such vortices explains why in the mass transfer profiles, the first minor, the second minor and the second major peaks (Fig. 4) of the highly turbulent flows are smaller than those of less turbulent flows. The decreased mass transfer rate with increase in *Re*

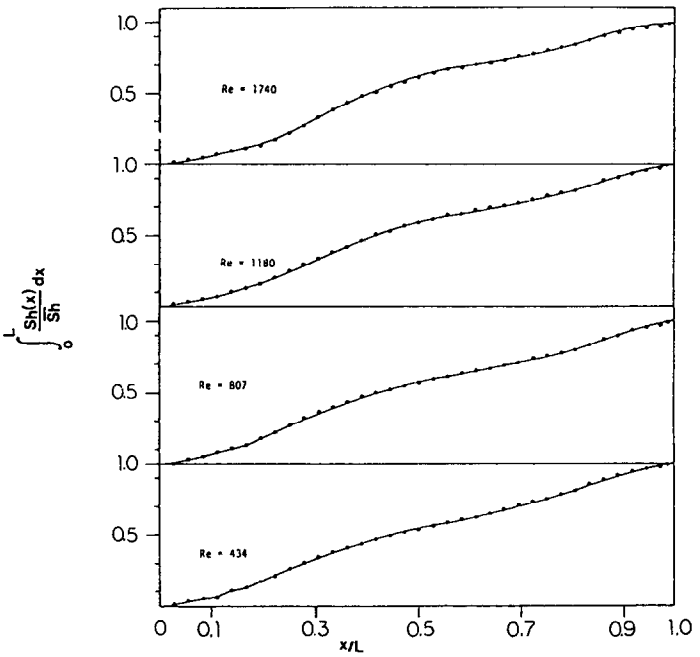

FIG. 9. The fractional cumulative contribution of the surface to the average mass transfer of the entire cylindrical surface. The value of *Sh* is an average of the point electrode over the entire surface.

in the second half of the surface ($\theta > 90°$) compensates for the increase in mass transfer rate on the first half. Thus the almost zero overall mass transfer dependence on *Re* in the turbulent regime.

Finally, the mass transfer rates in a packed bed and a pulsating flow trickle bed are reported to increase with *Re* in the turbulent regime. This behavior arises because the contact points between particles provide a far smaller relative surface area for recirculation flows with closed streamlines than the present trickle model. Thus while earlier experiments with a regular cubic array [18] clearly indicated flows with recirculations, the relative contribution of those areas which exhibit a near zero of negative mass transfer exponent dependence on *Re* is much smaller, resulting in *Re* dependencies which are near $n = 0.5$. Also, in packed beds, the sphere stagnation point may lie closer to 0°, thus engaging a larger share of the forward half of the sphere for mass transfer in the absence of recirculation mass transfer resistance.

We now examine the laminar flow regime more closely. Theoretically, the mass transfer coefficient over a flat plate is proportional to $Re^{0.5}$. Similarly, the mass transfer correlations in packed beds and trickle beds containing randomly packed spheres or short cylinders also have an *Re* exponent dependence of the same magnitude ($n \sim 0.5$). However, our experimental value of n is only 0.24 for the average Sherwood number (Table 1). The *Re* dependence of the local mass transfer varies with angular position. The value of n appears to be slightly lower at positions 20° and 35° where the stagnation point may appear. The dependence of the exponent is also low at the separation vortex (110°–150°), and n is actually negative at 120° and 130°. The small values from 70° to 100° appear to indicate that the laminar flow is progressively more retarded with increasing *Re* by the pressure gradient, consistent with the advance of the separation point with *Re*. The positions close to the contact points, 0° and 180°, are well insulated from the main film flow; a fact borne out by their extremely low *Re* dependence.

While the Leveque solution which applies to a fully developed boundary layer predicts

$$Sh = a\,Re^{1/3}\,Sc^{1/3} \tag{5}$$

it would not be logical to apply this relation to the incomplete boundary layer flow of the present experiment. The explanation lies in a boundary layer asymptotic solution for large *Re* and short contact time. Hirose *et al.* [27] showed that

$$Sh = a\,Re^{1/9}\,Sc^{1/3}. \tag{6}$$

Their experimental results for flow over large single spheres (19–76 mm diameter), and a later experiment [28] with flow over a single cylinder supported the above relation. But the experimental result becomes proportional to $Re^{1/3}$ as the flow rate increases beyond $Re = 58$, a result attributed to the appearance of surface waves. It is likely that such surface waves also arise due to exit effects from the single sphere or cylinder. Otherwise, a simple surface wave should not affect the boundary layer flow.

The minimum liquid superficial velocity of our experiment is about 0.10 m s^{-1}. On a particle surface 6 mm in diameter, the prediction of the short contact

time asymptote is more applicable to our results, at least in the region 40°–100°. It is also of interest to note that Satterfield *et al.* [10] have similarly observed a weak dependence on Re in a fully wetted gas continuous trickle bed and found that in this regime, Sh is proportional to $Re^{0.26}$.

Effect of gas flow rate

The gas flow rate has negligible observable effects on local mass transfer in the trickle flow model. The maximum cocurrent superficial velocity used was 2.1 m s^{-1}. Similar results were also obtained with countercurrent gas flow. The behavior of the trickle model is in accordance with the gross reactor behavior of an actual trickle bed reactor in a similar hydrodynamic regime [8, 10, 15, 29]. Even with higher gas superficial velocities in the blurring or mist gas continuous regimes, the liquid–solid mass transfer rate varies no more than 10% [10].

Comparison of mass transfer with trickle beds

An attempt is made here to assess how close the flow model approximates a trickle bed reactor in the trickle flow regime. The magnitude of the measured overall mass transfer coefficient, representative of convective mass transport, is in the range 6×10^{-5}–9×10^{-5} m s^{-1}, while the range for the local mass transfer coefficient is 4×10^{-5}–2.5×10^{-4} m s^{-1}. The local mass transfer rate measured with an electrochemical technique is usually expected to be higher than a packed bed of particles for which all are active in mass transfer, e.g. with the dissolution technique. For the same reason, it is expected that mass transfer studies involving a single particle offers a better opportunity to observe liquid–solid interaction [15, 17].

We have mentioned that in our results, the mass transfer dependence on Re is very weak. On the other hand, our data agree quite well with a short contact time asymptotic solution. In addition, our correlation of the overall mass transfer in the laminar flow regime, for the trickle rod column

$$Sh\,Sc^{-1/3} = 11.6Re^{0.24} \tag{7}$$

is in reasonable agreement with the trickle bed result [10] in the fully wetted gas continuous regime

$$Sh\,Sc^{-1/3} = 8.4Re_p^{0.26} \tag{8}$$

where Re_p is the liquid Reynolds number of a trickle bed based on the superficial velocity and packing diameter. To better compare the two correlations on a more consistent definition of Reynolds numbers, we can derive [8]

$$Re_p = 2Re/3(1-\varepsilon) \tag{9}$$

where ε is the void fraction of the bed. Further substitute equation (9) in equation (7) and choose $\varepsilon = 0.4$

$$Sh\,Sc^{-1/3} = 10.5Re_p^{0.24} \tag{10}$$

which is in fairly good agreement with correlation (8), considering the simplicity of the trickle model and the tendency of measurements on isolated packing to give higher mass transfer results than observed in a fully active bed.

CONCLUSION

The local mass transfer profiles and shear stress profiles exhibit large variations along the surface. As a result of the simplified geometry, our mass transfer profiles exhibit a very orderly change with Re over a large range. Together with the results of the isolated electrode, the detailed flow pattern over the cylindrical surface is justified. The result confirms features which are absent in numerical calculations [19, 29].

Acknowledgment—The author would like to thank D. F. Ollis for his support and encouragement throughout the course of this work.

REFERENCES

1. P. A. Ramachandran and R. V. Chaudhari, *Three-phase Catalytic Reactors*, pp. 200–255. Gordon and Breach, New York (1983).
2. M. P. Dudukovic and P. L. Mills (Editors), *Chemical and Catalytic Reactor Modeling*, ACS Symp. Ser., Vol. 237, pp. 3–84. American Chemical Society, Washington, D.C. (1984).
3. R. M. Koros, Engineering aspects of trickle bed reactors. In *Chemical Reactor Design and Technology* (Edited by H. I. de Lasa), pp. 579–630, NATO ASI Series. Martinus Nijhoff, Dordrecht (1986).
4. A. Gianetto and F. Berruti, Modelling of trickle bed reactors. In *Chemical Reactor Design and Technology* (Edited by H. I. de Lasa), pp. 631–685, NATO ASI Series. Martinus Nijhoff, Dordrecht (1986).
5. V. G. Rao, M. S. Ananth and Y. B. G. Varma, Hydrodynamics of two-phase cocurrent downflow through packed beds; Part I. Macroscopic model; Part II. Experiment and correlations, *A.I.Ch.E. Jl* **29,** 467–482 (1983).
6. G. Christensen, S. J. McGovern and S. Sundaresan, Cocurrent downflow of air and water in a two-dimensional packed column, *A.I.Ch.E. Jl* **32,** 1677–1689 (1986).
7. S. Goto, G. Levec and J. M. Smith, Mass transfer in packed beds with two-phase flow, *Ind. Engng Chem. Proc. Des. Dev.* **14,** 473–478 (1975).
8. T. Hirose, Y. Mori and Y. Sato, Liquid to particle mass transfer in fixed-bed reactor with cocurrent gas–liquid downflow, *J. Chem. Engng Japan* **9,** 220–225 (1976).
9. S. Morita and J. M. Smith, Mass transfer and contacting efficiency in a trickle bed reactor. *Ind. Engng Chem. Fund.* **17,** 113–120 (1978).
10. C. N. Satterfield, M. W. Van Eek and B. S. Bliss, Liquid–solid mass transfer in packed beds with downward cocurrent gas–liquid flow, *A.I.Ch.E. Jl* **24,** 709–717 (1978).
11. V. Specchia, G. Baldi and A. Gianetto, Solid–liquid mass transfer in concurrent two-phase flow through packed beds, *Ind. Engng Chem. Proc. Des. Dev.* **17,** 362–367 (1978).
12. N. D. Sylvester and P. Pitayagulsarn, Mass transfer for two-phase cocurrent downflow in a packed bed, *Ind. Engng Chem. Proc. Des. Dev.* **14,** 421–426 (1975).
13. J. A. Ruether, C. Yang and W. Hayduk, Particle mass transfer during cocurrent downward gas–liquid flow in packed beds, *Ind. Engng Chem. Proc. Des. Dev.* **19,** 103 107 (1980).

14. T. S. Chou, F. L. Worley and D. Luss, Local particle–liquid phase mass transfer; fluctuations in mixed-phase cocurrent downflow through a fixed bed in the pulsing regime, *Ind. Engng Chem. Fund.* **18,** 279–283 (1979).
15. V. G. Rao and A. A. H. Drinkenburg, Solid–liquid mass transfer in packed with cocurrent gas–liquid downflow, *A.I.Ch.E. Jl* **31,** 1059–1068 (1985).
16. Ch. B. Delaunay, A. Storck, A. Laurent and J. C. Charpentier, Electrochemical determination of liquid–solid mass transfer in a fixed bed irrigated gas–liquid reactor with downward co-current flow, *Int. Chem. Engng* **22,** 244–251 (1982).
17. K. R. Jolls and T. J. Hanratty, Use of electrochemical techniques to study mass transfer rates and local skin friction to a sphere in a dumped bed, *A.I.Ch.E. Jl* **15,** 199–205 (1969).
18. A. Karabelas, T. Wegner and T. Hanratty, Flow pattern in a close packed cubic array of spheres near the critical Reynolds number, *Chem. Engng Sci.* **28,** 673–682 (1973).
19. A. E. Saez, R. G. Carbonell and J. Levec, The hydrodynamics of trickling flow in packed beds. Part I: Conduit models, *A.I.Ch.E. Jl* **32,** 353–368 (1986).
20. A. Zukauskas and J. Ziugzda, *Heat Transfer of a Cylinder in Crossflow*. Hemisphere, London (1985).
21. H. E. Dukler and O. P. Bergelin, Characteristics of flow in falling liquid films, *Chem. Engng Prog.* **48,** 557–563 (1952).
22. G. D. Fulford, The flow of liquids in thin films, *Adv. Chem. Engng* **5,** 151–236 (1964).
23. A. Acrivos, On the solution of the convection equation in laminar boundary layer flows, *Chem. Engng Sci.* **17,** 457–465 (1962).
24. H. Schlichting, *Boundary Layer Theory*. McGraw-Hill, New York (1968).
25. V. G. Levich, *Physicochemical Hydrodynamics*, p. 102. Prentice Hall, Englewood Cliffs, New Jersey (1962).
26. V. G. Levich, *Physicochemical Hydrodynamics*, p. 34. Prentice Hall, Englewood Cliffs, New Jersey (1962).
27. T. Hirose, M. Toda and Y. Sato, Liquid phase mass transfer in packed bed reactor with cocurrent gas–liquid downflow, *J. Chem. Engng Japan* **7,** 187–192 (1974).
28. H. Miyashita, K. Saeki, H. Ueda and T. Mizushina, Transport phenomena in laminar flow of a liquid film on a horizontal cylinder, abstract, *J. Chem. Engng Japan* **8,** 511 (1975).
29. J. Deiber and W. Schowalter, Flow through tubes with sinusoidal axial variations in diameter, *A.I.Ch.E. Jl* **25,** 638–644 (1979).

MESURE DU TRANSFERT DE MASSE LOCAL LIQUIDE–SOLIDE DANS UN ECOULEMENT DE RUISSELLEMENT EN FILM; PAR UTILISATION DE LA TECHNIQUE ELECTROCHIMIQUE

Résumé—Un modèle de ruissellement en film bidimensionnel qui est une colonne verticale garnie de tiges horizontales est utilisé pour obtenir les caractéristiques du transfert de masse entre un gaz en écoulement continu et un film liquide dans un réacteur à ruissellement. Les taux de transfert de masse liquide–solide, locaux et globaux, sont déterminés par la technique du courant limite. La variation du nombre de Sherwood local avec la position angulaire est mesurée pour $400 < Re < 2000$. Par une méthode électrochimique unique de mesure du transfert de masse, on révèle l'existence de deux tourbillons derrière une séparation d'écoulement.

MESSUNG DES LOKALEN STOFFAUSTAUSCHES ZWISCHEN FLÜSSIGER UND FESTER PHASE IN EINER RIESELFILMSTRÖMUNG UNTER VERWENDUNG EINER ELEKTROCHEMISCHEN TECHNIK

Zusammenfassung—Mit Hilfe einer senkrechten Anordnung horizontaler Stäbe wird der Stoffaustausch zwischen flüssiger und fester Phase in einem Festbett-Reaktor mit voll benetzender Rieselfilm-Strömung und kontinuierlicher Gasphase untersucht. Der lokale und der mittlere Flüssig-Fest-Stoffaustausch wird dabei mit der Grenz-Strom-Technik bestimmt. Die lokale Sherwood-Zahl wird in Abhängigkeit von der Winkelposition im Bereich $400 < Re < 2000$ gemessen. Mit einem besonderen Verfahren zur elektrochemischen Messung des Stoffaustausches wird die Existenz zweier Wirbel hinter einer Strömungs-Separation gezeigt.

ИЗМЕРЕНИЕ ЛОКАЛЬНОГО МАССООБМЕНА ЖИДКОСТИ И ТВЕРДОГО ТЕЛА В МОДЕЛИ ТЕЧЕНИЯ СТЕКАЮЩЕЙ ПЛЕНКИ С ПОМОЩЬЮ ЭЛЕКТРОХИМИЧЕСКОГО МЕТОДА

Аннотация—С помощью двухмерной модели течения стекающей пленки, состоящей из вертикальной колонны, заполненной горизонтальными стержнями, рассчитаны характеристики массообмена между жидкостью и твердым телом в стекающей пленке жидкости, контактирующей с газом. Определены локальные и средние интенсивности массообмена. Методом предельного тока измерены локальные числа Шервуда при $400 < Re < 2000$. С помощью нового метода обработки данных измерения массообмена установлено существование двух вихрей за областью отрыва потока.